Charge Polarization at Catalytic Metal-Support Junctions

Part A: Kelvin Probe Force Microscopy Results of Noble Metal Nanoparticles

Tobias Kittel [1†] *and Emil Roduner* [1,2]*

[1] Institute of Physical Chemistry, University of Stuttgart,

Pfaffenwaldring 55, D-70569 Stuttgart, Germany

[2] Department of Chemistry, University of Pretoria, Pretoria 0002, Republic of South Africa

ABSTRACT

Metal oxide-supported nanoparticles of the platinum group metals Pt, Rh and Pd were studied at ambient temperature and atmosphere using Kelvin probe force microscopy. In all cases, the results reveal electron transfer from the metal to the oxide support which decreases in the order TiO_2 > CeO_2 >> Al_2O_3, leading to charge polarization at the Schottky type interfaces analogous to that of a parallel plane capacitor. This polarization cancels out to a large extent for the Kelvin signal. On top of this there is a much smaller number of positive charges at the outer catalyst particle surface, compensated by negative charges near the oxide surface. They show the same trend over the different oxides. These charges determine the constant electrical potential of the metal and are suggested to be the important component of the electronic catalytic metal-support interaction which are known to be much stronger for reducible than for non-reducible oxides.

KEYWORDS: Noble metal catalysis; metal oxide support; catalyst-support effect; charge polarization; Kelvin probe microscopy

INTRODUCTION

Oxide-supported noble metal particles are important solid state catalysts with applications in various reactions such as hydrogenations, dehydrogenations or skeletal isomerizations.[1] At a first glance, the support serves to disperse the expensive metal and provide large accessible surface areas of the catalytically active phase, but in reality, supported catalysts are extremely complex systems.[2] Size is an important parameter of the metal, not only because small particles have a large fraction of atoms at the surface, minimizing the fraction of 'useless' occluded atoms and thus providing a more economic use of the expensive noble metals. Rather, due to nano-size effects, the first ionization potential (IP) and the electron affinity (EA) change by several eV as a function of size, which is huge on a scale of chemically relevant thermal energies (typically a few tens of meV).[3] This is illustrated by the values of relevance in this work, i.e. those for the platinum atom, for which IP amounts to 9.0 eV and EA to 2.1 eV, while for the bulk metal both these properties assume the value of the work function, 5.3 eV. These properties determine the availability of electrons for redox reactions or for the formation of transient bonds to adsorbed substrates.[3] There is also a shape effect which describes the fact that substrate binding energies depend on the type of crystal facet. In particular, they generally increase with the extent of under-coordination from surface to edge and to corner sites of catalyst crystallites.[4] Furthermore, the existence of metal-support interactions is widely accepted in literature, but their exact nature is still under discussion.[5] They probably consist of several contributions, like promotion by specific cations in the immediate vicinity, or by the interaction with functional groups. Furthermore, one distinguishes between systems with reducible oxides like TiO_2 which exhibit strong metal support interactions (SMSI) and systems with weak metal-support interactions (WMSI) based on non-reducible oxides like SiO_2 and Al_2O_3.[2,6] The term SMSI was coined by Tauster *et al.* in studies of platinum group metals on TiO_2.[7,8] An understanding of these mutual interactions

between metal and support is of central importance for heterogeneous catalysis but has been impeded mostly by the difficulty to single out a contribution and study it separately from others.

However, metal nanoparticles are also known to interact with their metal oxide-semiconductor support by a mechanism akin to the Schottky effect, involving a charge transfer across the interface. This effect has often been proposed to account for variations in the catalytic behavior with changing nature of the support or the metal particle,[9] but in real systems it is often obscured by other parameters like particle shape and size distribution, the presence and concentration of other catalytic centers, promotors or surface poisoning, and by heterogeneities in space and time in general. Catalytic results are thus not normally of sufficient spatial resolution and not suited to discriminate between highly debated mechanistic models, and they do not provide the extent of charge transfer of metal-support interactions.[10-12] Only very recently, a combined XPS, STM and DFT study of small Pt clusters supported on CeO_2 derived the number of electrons transferred from the metal to the oxide.[13] In principle, Kelvin probe force microscopy (KPFM) has been used to address such questions, but measurements were mostly performed with single crystals under high vacuum, which is not the condition under which catalysis operates. Here we use KPFM with real catalysts in the form of powders in nitrogen/oxygen atmosphere under ambient pressure to investigate the charge polarization effects for Pt, Pd and Rh nanoparticles on CeO_2, and for Pt also on TiO_2 and Al_2O_3 oxide supports with a nominal resolution of a few nanometers.

Kelvin probe force microscopy, also known as surface potential microscopy, is a technique that combines the classical macroscopic Kelvin probe and a modern scanning probe microscope (SPM). A combination of an AC and a DC voltage is applied between the SPM tip and the back electrode (*i.e*. the metal sample holder) in non-contact mode in which the tip is scanned tracing the line of the topography scan at a constant height above the sample

surface. In this configuration, tip and sample effectively form a capacitor, and the detected signal is the compensating voltage as a function of the scanning coordinate.

Electric dipoles on the sample surface cause an additional electric potential at the position of the tip, and because of the applied AC voltage attracting and deflecting forces oscillate the tip. This force on the tip is approximately proportional to two terms: 1) the applied AC voltage to the tip and 2) the difference between applied DC voltage and the electrostatic potential caused by the sample. The first AC voltage term determines the sensitivity and the oscillation amplitude of the tip. The voltage difference term is set to zero during the measurement by setting the applied DC voltage equal to the electric potential caused by the sample to minimize the oscillation of the tip. A detailed description of the KPFM method in various applications is available in literature.[14]

The theoretical foundation of the method and the development of data analysis based on different models and exemplified for the typical case of a Pt particle on a TiO_2 support is given in a companion paper [15] and the full details are available in a PhD thesis which be accessed online.[16]

BACKGROUND

Nature of the Kelvin signal: The Kelvin probe signal is defined as the applied voltage that compensates the electrostatic potential above the sample surface. A negative signal means a positive electrostatic potential at the position of the tip which reflects an electric dipole moment pointing from the oxide support to the metal particle. Negative Kelvin probe signals on the metal therefore imply a transfer of negative charge from the metal particle to the underlying oxide support. This is the effect detected here, and it is in agreement with an UHV investigation by Sasahara *et al.*[17] who observed a transfer of negative charge from platinum particles with diameters ≤3 nm to the support, a TiO_2 single crystal surface. Independently,

the sign of the charge transfer was verified in the present work by measuring the known polarities [18] of the polycrystalline reflecting and the amorphous non-reflecting phases of a re-writable CD (CD-RW). Since the sign of the Kelvin potential is essential this experiment is shown in Figure S1 of the Electronic Supporting Information (ESI).

Metal-semiconductor junction and catalysis: A metal-semiconductor junction can be conductive and therefore non-rectifying, with an Ohmic resistance. Alternatively, it can be rectifying if there exists a contact barrier (the Schottky barrier) that is appreciably higher than the thermal energy, *kT*. The latter situation arises when the electrons in the conduction band of an *n*-type semiconductor are depleted or when the holes in the valence band of a *p*-type semiconductor are filled near the interface. This leads to a non-conductive layer in the semiconductor near the interface, and to charge polarization. The dependence of the Schottky barrier width and height on the size of metal nanoparticles determines the transport characteristics across the barrier.[19,20] The present experiments, however, relate to the situation where the charge transport has ended so that an equilibrated polarization is detected.

In catalysis, noble metal particles are commonly supported on various oxides, often SiO_2 or Al_2O_3, both of which have a high band gap and are nominally insulators. Other supports include TiO_2 which shows a particularly strong metal-support interaction [21] and CeO_2. Both are semiconductors with a band gap of 3.2 eV. As intrinsic, fully stoichiometric compounds, the electrical conductivity of all of these compounds would be rather minute near room temperature. However, oxides are rarely fully stoichiometric. Like silicon or other semiconductors of technical importance they can be doped intentionally with ions of a different valence, *e.g.* Fe(III).[22] However, far more frequent is non-intentional doping, with hydrogen being the most common impurity which is difficult to properly assign to the sample because of its abundance in the environment. As remnants from synthesis in aqueous environments or as a consequence of water uptake from the atmosphere it is typically present

in the form of HO^-, replacing one oxygen dianion and forcing a neighboring Ti(IV) or Ce(IV) metal ion (in the following abbreviated as Me(IV)) to change its oxidation state to Me(III). The Me(III) defect represents an excess electron which is located energetically slightly below the conduction band, as is typical for *n*-type semiconductors (compare Figure 1 of companion paper).[15] It can easily be promoted into the conduction band at thermal energies, or at the interface to a metal catalyst particle it can be transferred to the metal. If the Fermi energy of the metal is below the energy of these Ti(III) defects, as it is the case for Pt, this will lead to a depletion of the defect states, which is equivalent to a conversion of Ti(III) to Ti(IV) near the interface, and one expects a positive polarization of the corresponding semiconductor layer.

As it will be seen, the present experiments reveal the opposite sign of charge transfer, suggesting TiO_2 to behave like a p-type semiconductor. In the case of an oxygen terminated α-Al_2O_3 surface ab initio studies show a transfer of negative charge from supported platinum (111) films because of the slight electronegativity of an oxygen terminated surface.[23] If not heated out in vacuum under elevated temperature the surface of oxides tends to be terminated by hydroxyl groups. It is thus difficult to explain a negative semiconductor polarization under vacuum conditions. However, in oxygen atmosphere or in air, oxygen molecules may adsorb at the oxide surface and act as low energy traps for excess electrons, including those transferred from the metal particle. This leads to the formation of superoxide radical anions, $O_2^{\bullet -}$,[24,25] and it provides a possible mechanism for an explanation of the observed *p*-type behavior and the direction of polarization. The presence of electron donating metals may further support the formation of such species.

Alternatively, at low oxygen partial pressure, the oxide may lose oxygen in the form of O_2, leaving behind two oxide vacancies and four electrons per O_2 molecule. This also leads to *n*-type conductivity as described in the previous paragraph.

Many oxides equilibrate with atmospheric oxygen at ambient or elevated temperature. *Via* the described mechanism, this changes their electrical conductivity so that they can be used as oxygen sensors. The equilibrium of oxide adsorbed dioxygen plays a role also in reactions according to the Mars-van-Krevelen mechanism.[26]

In general, the defect chemistry of oxides is a complex issue that depends on the history of sample production, possibly with trapped non-equilibrium states. It is further a function of an environment which leads to water and oxygen uptake and release, in particular near the surface. The presence of supported metals and the conditions during catalysis can impose further complications. In the present work we have chosen to carry out the experiments under ambient atmosphere, in contrast to UHV conditions in literature work.

EXPERIMENTAL DETAILS

Sample Preparation: All samples were made via impregnation with aqueous metal salt solution.[27,28] Tetraamineplatinum-(II)-chloride, tetraaminepalladium-(II)-chloride and rhodium-(III)-trichloride, cerium dioxide (specified average grain size 5 μm) and titanium dioxide (44 μm) were purchased from Sigma Aldrich, aluminum oxide (105-125 μm) was obtained from Fluka.

The metal oxide powder was suspended in doubly distilled water and subsequently mixed with metal salt solution with a metal content of 10 mg mL^{-1} to give a suspension containing 8 mL of the solution per gram of metal oxide.[27,28] The mixture was stirred at 80°C for four hours in a rotary evaporator, followed by evaporation of the water and drying of the impregnated samples overnight in the oven at 120°C. This procedure ensures that the added metal is deposited completely on the support to give the desired metal loading. Calcination and activation were carried out in a quartz glass flow reactor. For calcination the sample was heated up to 400°C under a flow of 120 mL min^{-1} of oxygen gas with a heating rate of

0.5 K min^{-1}, and it was kept at this temperature for 4 hours. After purging the oxygen by flowing nitrogen gas the sample was activated at 350°C for three hours in a flow of 30 mL min^{-1} hydrogen gas.

Scanning Probe Microscopy: For the measurements the powder was filled into a sample holder and slightly compressed to obtain a macroscopically flat surface. Sufficiently large oxide powder grains with an approximately horizontal crystal facet were selected for the measurements. SPM data were recorded using a Veeco Dimension™ D3100 instrument equipped with a Quadrex™ PhaseImaging™ module under ambient atmosphere and temperature. Nanoworld commercial PtIr5-coated silicon tips of 10-15 μm tip height with a resonant frequency of 75 kHz and a force constant of 2.8 N m^{-1} were used for all measurements. Because of the coating the typical curvature of fresh tips was as much as ~25 nm. For consistency, all images of a given metal-support combination which are reported here were measured with the same tip. For a new combination a fresh tip of the same type was used.

Both, topography and Kelvin imaging were performed by a two-pass (trace and retrace) technique. The topographical information was obtained in tapping mode. Normally, only the second path (reverse direction) of the Kelvin signal in constant height above the sample surface is stored. The scan height during this second pass is the average height during tapping mode, determined by the amplitude set point and the cantilever sensitivity. Usual scan heights above the sample surface were between 5 and 7 nm, and for each sample AC voltage and scan height were optimized for maximum sensitivity.

Data Analysis: Data imaging was performed using the free WsXM software [29] and the maximum of 512×512 points. This gives in all measurements at least 6 points per nm, which is much better than the real resolution that is limited by the tip radius of ~25 nm. All Kelvin

measurements are displayed relative to the support signal, which allows seeing directly the contribution caused by the particles.

The theoretical potential function was calculated in the fits using the *Matlab* software. When appropriate the analytical solutions (Eqns. 11-13 of companion paper)[15] were used, otherwise it was calculated numerically (Eqns. 7-9 of companion paper)[15] which was much more time consuming. Further details are given elsewhere.[16]

RESULTS AND DISCUSSION

Aluminum oxide (Al_2O_3, alumina), titanium oxide (TiO_2, titania (anatase)) and cerium oxide (CeO_2, ceria) powders were chosen as supports with a platinum loading of 1 wt% on alumina and titania and 2 wt% on ceria. Topography and surface potential images for the different oxide supports and corresponding profiles recorded under air at ambient pressure and temperature are shown in Figures 1-4 for Pt and in Figures 5 and 6 for Pd and Rh.

Topography: All topography images give evidence of separated particles on the surface. The observed Pt particle diameters range between 50 nm and 180 nm, the heights are up to 20 nm, which means the height is about one tenth of the width and one particle contains on the order of 10^{16} atoms. With 80 nm to 300 nm diameters, the Pd and Rh particles are larger than and also not as flat as those of Pt. All particles have their maximum height near their center. While aluminum oxide and titanium oxide surfaces support flattened hemispherical platinum particles, the Pt particles on cerium oxide look volcano shaped with a non-circular circumference, which may be the result of a sharper tip. The tip normally leads to an additional broadening of the actual particle shape, in particular for steep sample topographies (see Figure S4 of ESI).[30] The Pd and Rh particles are of less regular shape.

Experimental Surface Potential: Images of the Kelvin signal are shown in Figures 1-6. A lower signal-to-noise ratio in the case of alumina and titania samples compared to the ceria

sample is explained by the lower AC voltage of 3 V instead of 6 V that is applied to the tip, which causes a smaller deflection of the tip as well as a lower risk of touching the surface, but it reduces signal sensitivity. In the case of Pt/alumina the noise appears enhanced because of the small signal. All images show negative signals at the positions of the metal particles, which is equivalent of a positive electrostatic potential and reveals a transfer of electron density from the metal to the support. A more detailed inspection shows that for TiO_2 there is a change of sign of the Kelvin signal just outside the rim of the particle. It is better seen at higher resolution in Figure 3 (arrow). This halo in the Kelvin signal lies slightly outside a similar halo in the topography signal which probably represents the foot of the particle. Between the particles, some grooves are seen which correspond to higher values of the Kelvin signal. They may represent grain boundaries on the surface of the polycrystalline support. Furthermore, the Figures 1 and 2 show that the surface potential signals for Pt on titania and ceria are higher by two orders of magnitude compared to those obtained on the alumina support in Figure 4. Those for Pd and Rh on ceria are intermediate (Figures 5, 6). This demonstrates that the Kelvin signal depends strongly on both, the support and the metal.

Comparison of the topography and the Kelvin probe signal shows that the two are close to antisymmetric, *i.e.* higher particles show a more negative signal. The Kelvin probe signals are also somewhat broader than the particles. Furthermore, a shift of the Kelvin probe signal depends on the thickness of the tip and is an artifact of the trace-retrace data acquisition technique (see ESI, Figure S4). Along the scanning direction of the tip the signal shifts to higher x-values by up to 26 nm (trace) and –17 nm (retrace).

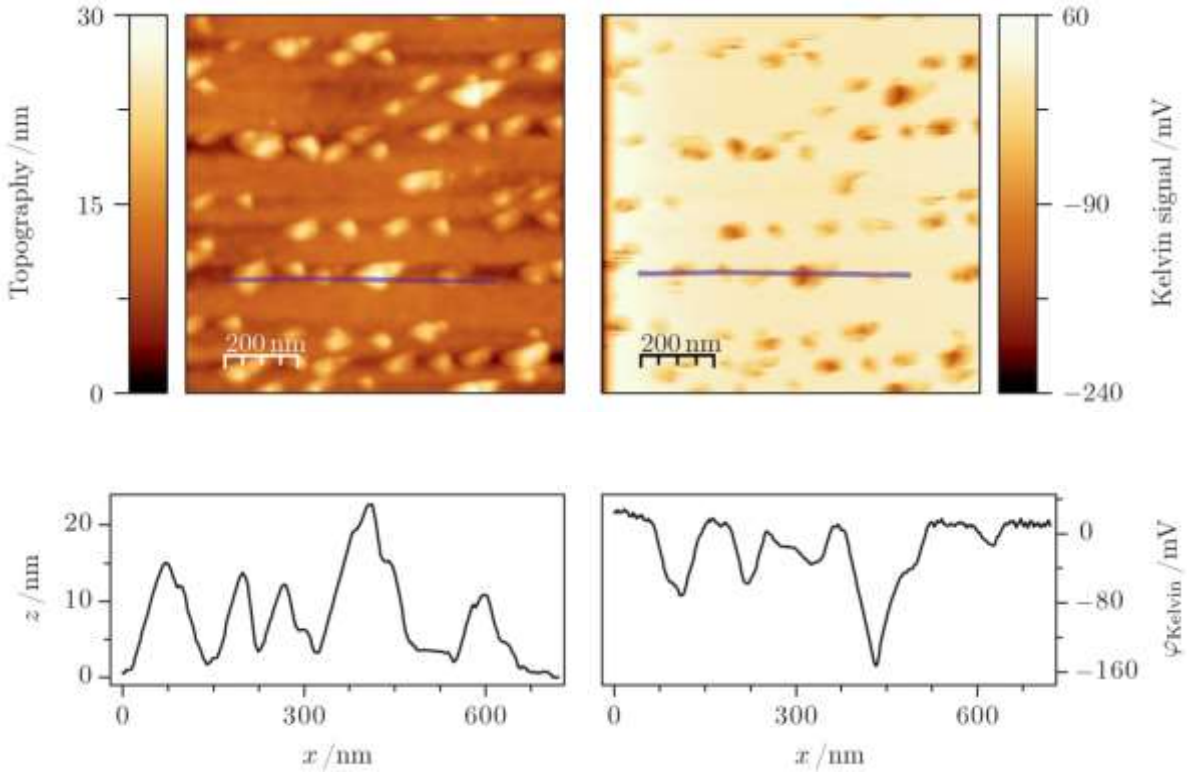

Figure 1. Experimental topography image (left) and Kelvin probe signal (right) for 2wt% Pt/CeO_2. The profiles below the full images are taken along the green line in the full image. Measurements were conducted in tapping mode with amplitude set value of 0.3 V and in Kelvin probe mode with an AC voltage of 6 V.

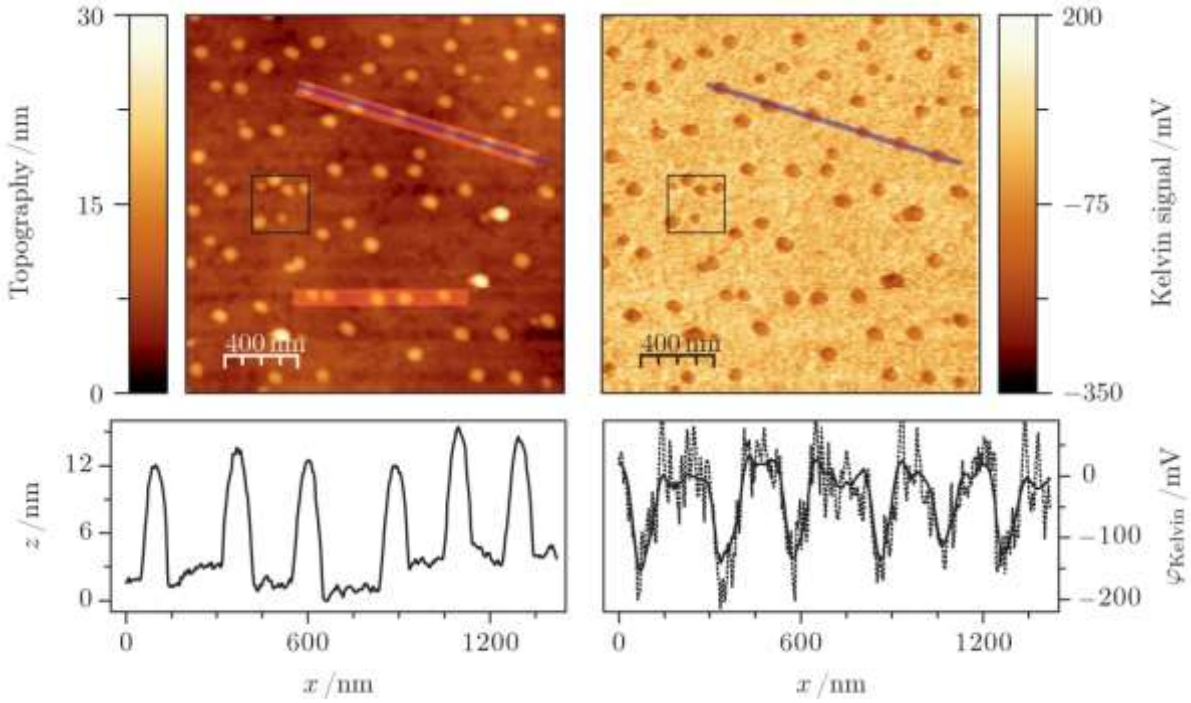

Figure 2. Experimental topography image (left) and Kelvin probe signal (right) for 1wt% Pt/TiO_2. The profiles below the full images are taken along the line in the full image. Measurements were conducted in tapping mode with amplitude set value of 0.3 V and in Kelvin probe mode with an AC voltage of 3 V.

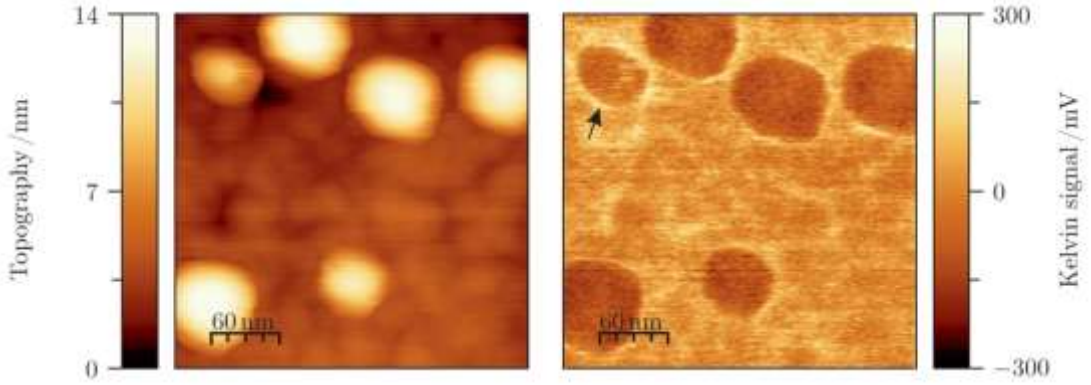

Figure 3. Enhanced resolution experimental topography image (left) and Kelvin probe signal (right) for 1wt% Pt/TiO_2. The images represent separate measurements corresponding to the square shown in Figure 2. The arrow points to the potential trough around the rim of the particles.

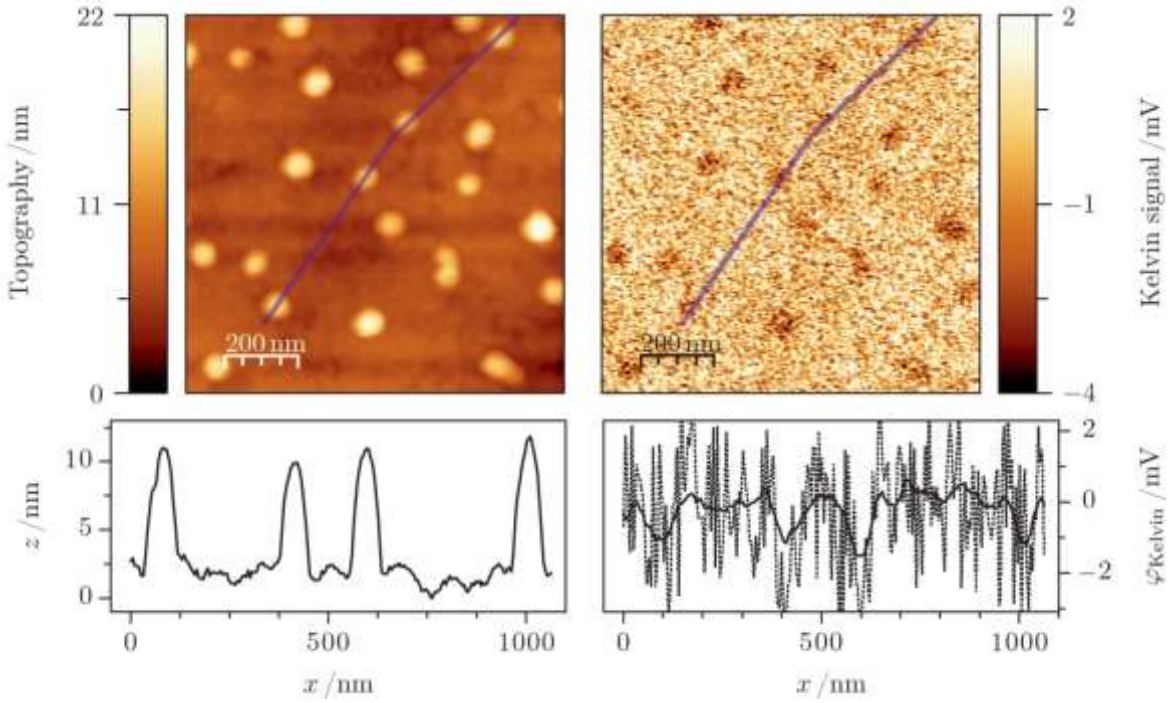

Figure 4. Experimental topography image (left) and Kelvin probe signal (right) for 1wt% Pt/Al_2O_3. The profiles below the full images are taken along the green line in the full image. Measurements were conducted in tapping mode with amplitude set value of 0.45 V and in Kelvin probe mode with an AC voltage of 3 V.

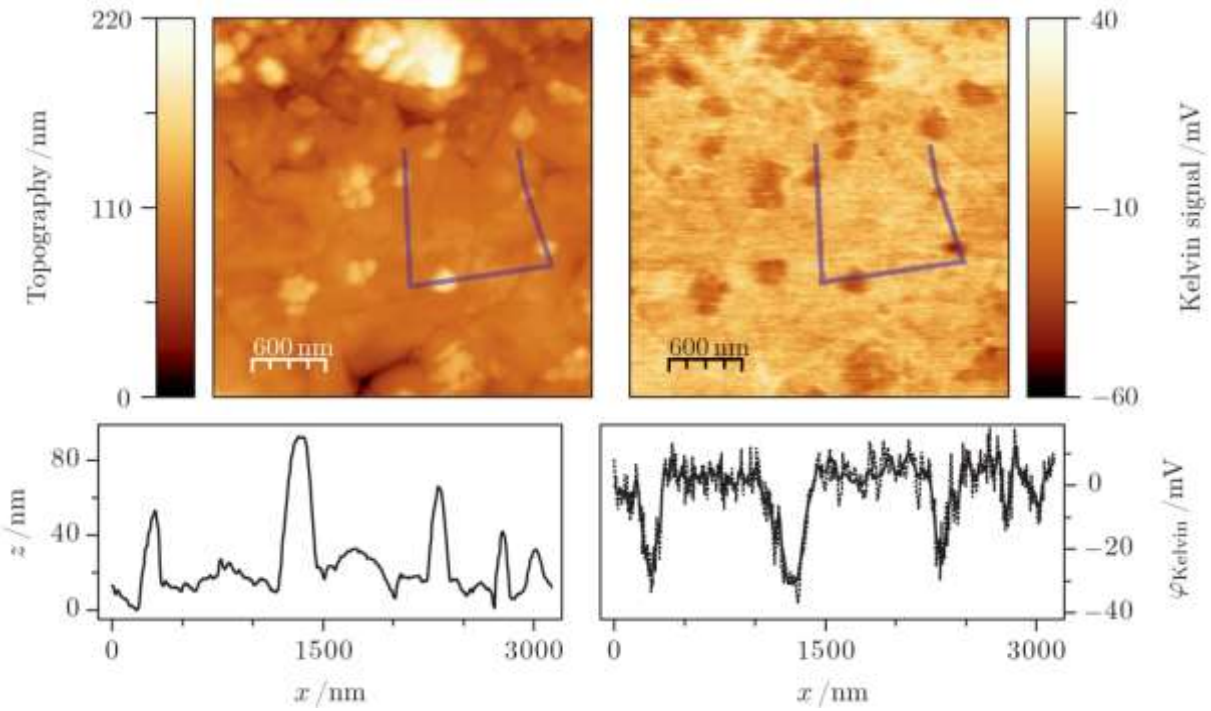

Figure 5. Experimental topography image (left) and Kelvin probe signal (right) for 1wt% Pd/CeO_2. The profiles below the full images are taken along the green line in the full image. Measurements were conducted in tapping mode with amplitude set value of 0.4 V and in Kelvin probe mode with an AC voltage of 2 V.

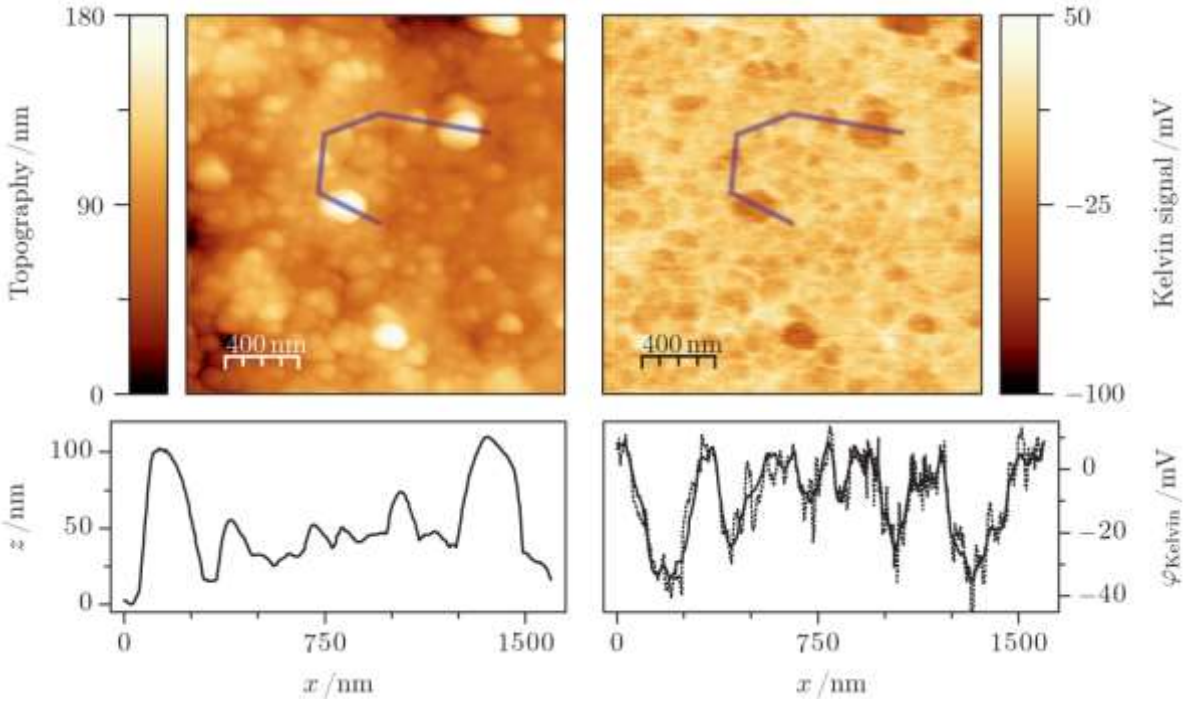

Figure 6. Experimental topography image (left) and Kelvin probe signal (right) for 1wt% Rh/CeO_2. The profiles below the full images are taken along the green line in the full image. Measurements were conducted in tapping mode with amplitude set value of 0.5 V and in Kelvin probe mode with an AC voltage of 2 V.

An increase of the Kelvin signal with particle diameter is observed for all samples, as shown in Figure 7 for the measured metals and supports. The dependence is particularly pronounced for Pt/TiO_2. The observed behavior suggests that the amount of transferred charge increases with true particle size, which agrees with observations of Pt/TiO_2 under UHV conditions.[32-34] A similar correlation is observed with the particle height (not shown). The interpretation must be done with care because the observed potential depends on the distance between the tip and the deficit charges in the metal particle and the excess charges in the support, *i.e.* on the location of the charges near the interface or on the particle surface and deeper in the bulk of the supporting oxide. The question is also whether the measured values reflect the different volumes or the different areas of the interface or whether there is in

addition a change in charge density (see Ref. 11 for the models which take these variables into account).

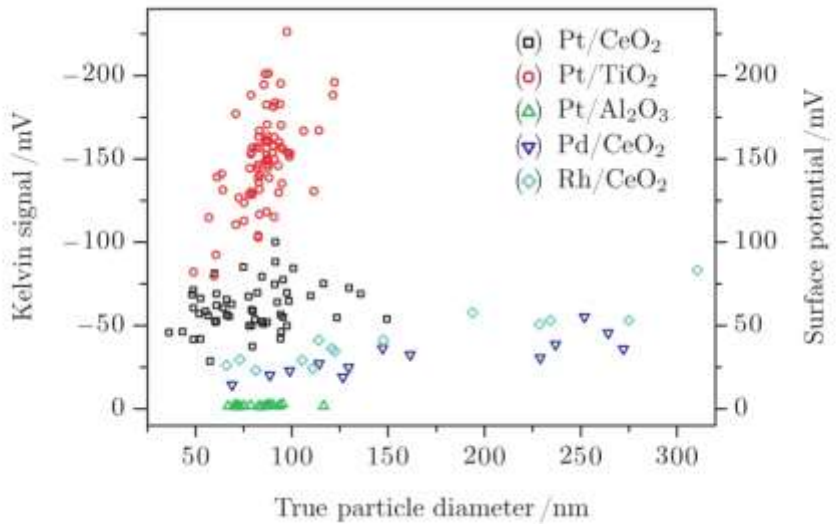

Figure 7. Maximum value of the Kelvin probe signal in dependence of the true particle diameter, *i.e.* after correction for broadening due to the finite tip radius (see ESI, Figure S4).

Simulations of the surface potential: The theoretical background of the simulations, the simulation procedure and their applications to the analysis of model particles is explained in a companion paper.[15] In all cases the potential of charge carriers is assumed to be constant over the conductive metal particle. Three profiles were evaluated to describe the particle shapes: a cone, a truncated ellipsoid, and a truncated paraboloid. The paraboloid proved to provide the most accurate description of the experimental particle shapes, and it leads to the best description of the observed Kelvin signal. It is therefore the only particle shape for which results are reported here. For the same reason of better agreement with experiment a hemispherical charge distribution in the support was discounted and only a planar distribution considered for further analysis.

A first model for the description of the charge distributions derives from a simple planar capacitor. It was developed by Sasahara *et al.*[33] and assumes a charge transfer across the

particle-support interface that results in a positive charge distribution which is exactly antisymmetric relative to the negative charge, at first without specifying the direction of charge transfer. These two charge density distributions represent a dipole that interacts electrostatically with the tip above the sample. This simple model did not lead to satisfactory agreement with the measured Kelvin probe signal.[15]

More sophisticated is the Schottky contact model of Hägglund and Zhdanov [34] which assumes in addition of the charges on both sides of the interface also charges at the external particle surface and the support surface in the neighborhood of the particle (Figure 3 of Ref. 12). These are varied numerically until a constant potential is reached inside the metal particle. The results confirm that the charge polarization represents an electron transfer from the metal to the support, which is equivalent to the effect of a metal catalyst on a *p*-type semiconductor support. Table 1 gives important fixed parameters which are used in the simulations of the different metal-support combinations. The simulations were carried out for the five samples with a total of ~180 particles using a pre-fixed charge density ρ_S in the support which was determined as described in the companion paper.[15]

Figure 8 summarizes the results of the simulations for charges and the derived charge densities as a function of the true (*i.e.* corrected, see Figure S4 of ESI) particle size R^* for all five systems. The size effects are most pronounced for Pt/TiO_2 and least pronounced for Pt on Al_2O_3. For all systems, the charges increase with R^*, but the homogeneous charge *densities* per unit area decrease slightly, indicating that the assumption of a homogeneous two-dimensional charge distribution describes the situation well. An exception is the charge on the outer particle surface, ρ_{OS} (OS for outer surface), which increases approximately linearly with R^*, indicating that the charges may be more confined along the particle circumference at the interface.

Table 1: Parameters used for quantitative Schottky contact model analysis (see accompanying paper),[12] and for comparison cation/metal atom density in first layer at the interface

sample	ε_S [a]	d [b]	h_{tip} [c]	ρ_S [d]	ρ(C) [e]	ρ(M) [f]
		/pm	/nm	/e nm^{-2}	/nm^{-2}	/nm^{-2}
Pt/TiO_2	110	200	5.1	–0.020	11.3	44.8
Pt/CeO_2	7	236	5.1	–0.010	7.9	44.8
Pd/CeO_2	7	235	6.7	–0.010	7.9	45.5
Rh/CeO_2	7	232	8.8	–0.010	7.9	47.5
Pt/Al_2O_3	9	193	7.2	–0.0002	16.7	44.8

a) Relative electrical permittivity of supporting oxide

b) Distance between planar charge zones at interface given by the sum of the metallic radius of the noble metal atom and of the ionic radius of the support cation

c) The average distance of tip above sample, h_{tip}, is equal to the tapping height

d) Homogeneous charge density in support used as a pre-fixed value in the analysis (see companion paper)[15]

e) Area density of support cations at interface, calculated for the (111) crystal face of alumina and ceria and the (101) crystal face of titania

f) Area density of metal atoms at the interface, calculated from lattice constant for a cubic dense packing of the metal

The height of the Pt particles extends up to about 20 nm, those of Pd and Rh are higher by a factor of 4-5. The diameter of the Pt particles is up to 150 nm, those of Pd and Rh reach double of this value. It is therefore a question whether quantum size effects which are normally restricted to below 100 nm play a role for the height. The Pt particles are relatively flat discs, and only their height is in the nano-range, in the other two dimensions they should

be considered bulk metals. The small height has the effect that as a function of energy the density of states increases in steps corresponding to the quantization in the short dimension. The net effect is that the ionization potential of the metal increases somewhat and becomes more atom-like.[4] This would make it more difficult for the smallest particles to transfer electrons to the support, which is basically compatible with observation. However, a nano-size effect is expected to flatten out towards bulk dimensions, exhibiting an inverse proportionality with dimension. Figure 8 shows the charge polarization scaling somewhat less than with the area of the interface but not with volume. This is not compatible with a quantum-size effect.

The extra charge on the external particle surface, Q_{OS}, is smaller by two orders of magnitude than that on the two sides of the interface, and it amounts to only up to 6 positive electron charges on any of the particles which were evaluated. For particles with $R^* > 150$ nm ρ_{OS} approaches zero, and the charges on the two sides of the interface compensate each other, as in a classical macroscopic capacitor. In contrast, edge effects become more important for the microscopic Schottky contact.

The extended charge regime of the support relative to the true particle radius, R_S/R^*, reaches nearly 200% for Pt/TiO_2, while it amounts to <125% for the other systems. These results derive from the best match of simulated and experimental Kelvin signals. Most significantly, the simulations reproduce the circular trough around the particle that is seen for Pt/TiO_2 (Figure 3, see also Figure 7 of Ref. 11). Reproduction of this trough is quite specific for the model that is chosen for the simulations. The simulations predict a weak trough signal also for the other systems where it is not discerned in the experiment, perhaps because of insufficient resolution.

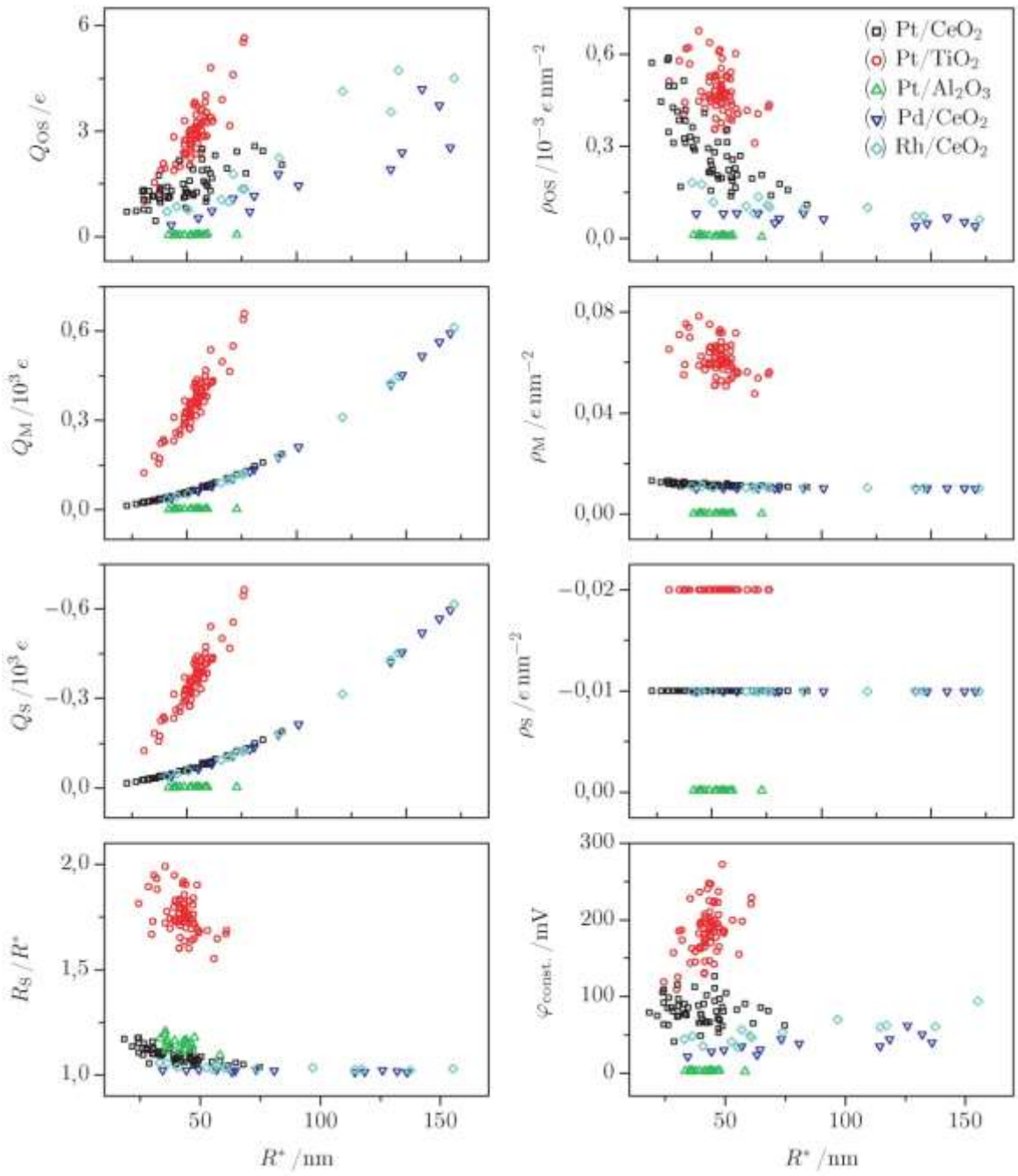

Figure 8. Charges Q_i and corresponding charge densities ρ_i resulting from simulations using the Schottky contact model with planar charge zones at both sides of the interface (Q_M and Q_S corresponding to ρ_M and ρ_S) and with fixed area charge density ρ_S in the support, and additional charges at the outer particle surface, Q_{OS}, and Q_S extending onto the support for $R^* \leq r \leq R_S$. The entries are for all systems and all evaluated particles as a function of the true particle radius R^*. Also shown is the resulting constant potential φ_{const} in the metal.

Interpretation of charge transfer and its dependence on the nature of metal and support: The present work shows convincingly that in all cases there is a polarization of the metal-support interface with transfer of electron density from the metal to the support. The largest effect is found for Pt/TiO_2, followed by equal polarizations of Pt, Pd and Rh on CeO_2; the smallest effect is found for Pt/Al_2O_3. Following the determination as described in the companion paper (Ref. 15) the interfacial polarization is taken to be equal for the different metals on CeO_2 since it is assumed that the extent of electron transfer is controlled by the available density of defects, ρ_S,. (–0.010 nm^{-2}, which is equivalent to one defect per 790 Ce cations in the first layer near the interface) in the support oxide near the interface. The defect density for TiO_2 was determined to be a factor 2 higher (–0.020 nm^{-2}). Interestingly, quite similar absolute values (0.035 and 1.2 nm^{-2}) were quoted in literature for Pt/TiO_2, although this was based on impedance spectroscopy, assuming electron conductivity in TiO_2,[35] but the most recent determination by XPS reported a charge transfer in the same direction for Pt/CeO_2 of 1.2 nm^{-2} in the limit of large nanoparticles.[13] This is two orders of magnitude more than in the present work, but it was obtained under quite different preparation and measurement conditions, and the support was a CeO_2 film of only 2.1 nm thickness supported on Cu(111). For such a thin film it is difficult to exclude an influence of Cu on the oxide. A very small but still negative value of only –0.00020 nm^{-2} was determined here for Al_2O_3.

For Pt/TiO_2, literature work reports [36] or assumes [37] electron transfer from the support to the metal but also the reverse way,[33] whereas no significant transfer was detected elsewhere for a pre-reduced sample.[21] For Au on TiO_2 terminated $SrTiO_3$ the electron transfer was from Au to TiO_2, no matter whether the support was stoichiometric, pseudo-stoichiometric or reduced.[37]

Following the catalyst preparation used in the present work with hydrogen reduction at 623 K one would normally expect an *n*-type TiO_2 semiconductor in which one hydrogen molecule reduces two Ti(IV) centers to Ti(III) and protonates two O^{2-} ions to HO^-. As shown in Figure

S2, isolated Ti(III) defects are located energetically only 0.09 eV below the lower edge of the conduction band and roughly 1 eV above the Fermi level of Pt (Figure S3). For this situation we expect the Ti(III) centers to transfer their excess charge to the Pt particle, which is in contradiction to our observation and to that of Ref. 33. However, as shown in the companion paper,[16] electron-hole pairs are stabilized by Coulomb interaction of *ca*. 2.5 eV across the interface, which is sufficient to reverse the situation. For the present work in air, isolated additional negative charges can be explained by support-adsorbed O_2 which can act as a low energy trap for excess electrons including those transferred from the metal. The work by Sasahara *et al*.[33] was performed in vacuum, and the stabilized electron hole pairs provide a consistent explanation with observations. For CeO_2, Ce(IV) can be reduced to Ce(III), and the energetic situation is very similar to that of TiO_2. Al_2O_3 is a very stable insulator with a wide band gap, but the lower edge of the conduction band is below the Fermi energy of the Pt particle (see Figure S3 of the ESI). This means that the Pt conduction electrons are free to move between metal and support so that they leave little observable difference between the two regimes. The fact that the Kelvin signal is much smaller than for the other supports is thus consistent with this band structure. The weak signal is also in line with the classification of Al_2O_3 as a non-reducible oxide which shows only weak metal-support interactions (WMSI), while TiO_2 and CeO_2 are reducible and show much stronger interactions (SMSI).[6]

As discussed above, nanosize effects are expected to be small since most particles are >50 nm in diameter. Related to this is the constant electrical potential inside the metal, φ_{const}. The largest value is found for Pt/TiO_2 (186 mV in the average over all evaluated particles), followed by a second range of polarizations for Pt (79 mV), Pd (39 mV) and Rh (56 mV) on CeO_2; the smallest effect is found for Pt/Al_2O_3 (39 mV). It should be noted that these are at first relative values which describe differences between metal and support. In a series where either the metal or the support are identical the numbers gain in relevance, but since a signal is

observed only in the presence of charge polarization the absence of a signal may be taken as a suitable reference equivalent of a free (unsupported) cluster.

The sign of φ_{const} is positive, independent of whether the analysis is based on a *p*-type or an *n*-type oxide support. This reflects the fact that the Kelvin potential is negative. The effect of charges of the capacitive electron-hole pairs about the interface cancels to a large extent in φ_{const}. We therefore conclude that the charges at the interface are not relevant for φ_{const} and therefore also not for the catalyst-support interaction. Instead, within the present model, it is the very few charges at the outer catalyst surface, Q_{OS}, which determine φ_{const} and which are thus the relevant property that describes the metal-support effect in catalysis.

For the same support, CeO_2, the Kelvin signal is largest for Pt which is the metal with the highest work function (5.64 eV) and electron affinity (2.15 eV). It is considerably less for Rh and again slightly less for Pd which have work function values of 4.98 and 5.22 eV and electron affinities of 1.14 eV and 0.56 eV, respectively. Neither the electron affinity which is an atomic property nor the bulk work functions show the expected correlations with φ_{const}. In fact, Pt is the most noble of these elements on both scales and should be the first that is neutral, and yet it reveals the opposite behavior with the highest positive charge density. The finding is not understood at this point, but it should be reminded that under the given conditions the surface even of a noble metal is not always a blank metal. After reduction in hydrogen it may be covered by chemisorbed hydrogen [38] or if exposed to air it may be contaminated with oxygen species. In particular, it has also been reported that after hydrogen reduction the metal of Ru/TiO_2 and other titania-supported noble metal catalysts are covered to a substantial degree with a titania overlayer and that this affects the turnover number considerably.[39] In other experiments, Pt particles were encapsulated by a FeO layed derived from the support.[5] That surface-adsorbed oxygen can change the properties of the oxide has already been discussed, but also the properties of the metal are sensitive to adsorbates. Each

chemisorbed hydrogen atom binds one of the conduction electrons and accumulates some negative charge because of the hydride like nature of these atoms. Oxide overlayers may be prone to defects and therefore have different acceptor properties. It therefore has to be kept in mind that any exposure to a gaseous environment may affect the nature of the surface compared with vacuum conditions, and this may therefore change the Kelvin probe signal.

The present work reports a proof of principle and the experimental development and theoretical analysis of the application of KPFM in studies of catalysis. So far, all experiments were performed at room temperature in ambient atmosphere. The real benefit of the method is expected to be in future in-situ or in-operando studies where temperature and gas atmosphere will correspond to catalytically relevant conditions.

CONCLUSIONS

- KPFM is a suitable experimental method to map the electrostatic surface potential of supported metal particles on a metal oxide support. All particles of our measurements show a negative Kelvin signal relative to the support. This corresponds to a positive electrostatic potential and to a transfer of negative charge from the noble metal particle to the metal oxide.
- For the same metal (Pt) the Kelvin signal is largest in the TiO_2 support, followed by CeO_2, and much smaller for Al_2O_3. This sequence is in agreement with the known fact that reducible oxide supports show much stronger metal-support interactions (SMSI) than non-reducible oxides. The small signal with alumina represents a weak metal-support interaction (WMSI), related to the energy of the lower edge of the conduction band which is slightly below the Fermi level of Pt so that electrons are expected to be freely mobile between support donor states and metal.

- Zero Kelvin signal means zero charge polarization and thus zero metal-support interaction. In this case the metal particle should behave like the unsupported (free) catalyst particle.
- Under the assumption of a constant electrical potential inside the metal the charge polarization represents mostly planar charge distributions on both sides of the interface which compensate each other in their effect on the constant potential in the metal.
- Much less positive charge is found at the outside surface of the metal particle but, depending on the simulation model, it is compensated by corresponding negative charge in the first layer of the support outside the rim of the particle. It is this positive charge on the particle surface which determines the constant potential in the metal that is responsible for the metal-support interaction.
- Unexpectedly, the polarization with the highest positive charge density on the metal particle is found for the most noble metal, *i.e.* for Pt. Possibly, this is related to surface contamination of the metal with chemisorbed hydrogen, oxygen, or to titania overlayers as has been reported previously.[39]
- The charge polarization of the metal particle may have an effect analogous to the application of an electrical potential in an electrochemical reaction.

Supporting Information. Details of the calibration of the sign of the signal and of the electronic band structures and energies of the materials are provided in supporting information. This material is available free of charge via the Internet at http://pubs.acs.org.

AUTHOR INFORMATION

* Corresponding author: e.roduner@ipc.uni-stuttgart.de, Phone: +27 12 420 4474

† Present address: Ontorix GmbH, Boschstraße 10, D-73734 Esslingen am Neckar, Germany

Author Contributions:

The manuscript was written through contributions of all authors. All authors have given approval to the final version of the manuscript. TK has conducted the experiment and designed and performed the analysis. ER has conceived and supervised the work.

ACKNOWLEDGMENTS

The work was performed within the Collaborative Research Center SFB 706 (Selective catalytic oxidations using molecular oxygen) in Stuttgart and funded by the German Research Foundation (DFG).

REFERENCES

1) Knözinger, H.; Kochloefl, K. Heterogeneous Catalysis and Solid Catalysts, in *Ullmann's Encyclopedia of Industrial Chemistry,* Wiley-VCH, Weinheim, 2005.

2) Ruppert, A. M.; Weckhuysen B. M.; Metal-Support Interactions, in *Handbook of Heterogeneous Catalysis*, (Ertl, G.; Knöziger, H.; Schüth, F., Weitkamp. J., Eds.) Wiley-VCH, Weinheim, 2008, 1178-1188.

3) Roduner, E. Size Matters: Why Nanomaterials Are Different. *Chem. Soc. Rev.* **2006**, *35*, 583-592.

4) Roduner, E. *Nanoscopic Materials: Size-Dependent Phenomena and Growth Principles*. Royal Society of Chemistry, Cambridge, 2014.

5) Willinger, M. G.; Zhang, W.; Bondarchuk, O.; Shaikhutdinov, S.; Freund, H.-J.; Schlögl, R. A Case of Strong Metal-Support Interactions: Combining Advanced

Microscopy and Model Systems to Elucidate the Atomic Structure of Interfaces. *Angew. Chem. Int. Ed.* **2014**, *53*, 5998-6001.

6) Bond, G. C. *Metal-Catalyzed Reactions of Hydrocarbons*, Series on Fundamental and Applied Catalysis (Twigg, M. V.; Spencer, M. S., Eds.) Springer, Berlin, **2005**.

7) Tauster, S. J., Fung, S. C., Garten, R. L. Strong Metal-Support Interactions – Group 8 Noble Metals Supported on TiO_2. *J. Amer. Chem. Soc.* **1978**, *100*, 170-175.

8) Tauster, S. J., Fung, S. C., Stong Metal-Support Interactions – Occurrence Among Binary Oxides of Groups IIa-IVb, *J. Catal.* **1978**, *55*, 29-35.

9) Ioannides, T.; Verykios, X. E. Charge Transfer in Metal Catalysts Supported on Doped TiO_2: A Theoretical Approach Based on Metal-Semiconductor Contact Theory. *J. Catal.* **1996**, *161*, 560–569.

10) Zhdanov, V. P. Nm-Size Metal Particles on a Semiconductor Surface, Schottky Model etc. *Surf. Sci.* **2002**, *512*, L331–L334.

11) Ioannides, T. Comment on: "Nm-Size Metal Particles on a Semiconductor Surface, Schottky Model etc." *Surf. Sci.* **2003**, *530*, 216–218.

12) Zhdanov, V. P. Reply to comment on "Nm-Size Metal Particles on a Semiconductor Surface, Schottky Model etc." *Surf. Sci.* **2003**, *530*, 219–220.

13) Lykhach, Y.; Kozlov, S. M.; Skála, T.; Tovt, A.; Stetsovich, V.; Tsud, N.; Dvořák, F.; Johánek, V.; Neitzel, A.; Mysliveček, J.; et al. Counting Electrons on Supporting Nanoparticles. *Nature Mat.* **2015**, *15*, 284-288.

14) Melitz, W.; Shen, J.; Kummel, A. C.; Lee, S. Kelvin Probe Force Microscopy and its Application, *Surf. Sci. Rep.* **2011**, *66*, 1-27.

15) Kittel, T.; Roduner, E.; Charge Polarization at Catalytic Metal-Support Junctions. Part B: Theoretical Modeling of Kelvin Probe Force Microscopy Experiments. *J. Phys. Chem. C* (companion paper).

16) T. Kittel, *Untersuchung von Edelmetallpartikeln auf Metalloxidträgern mittels Kelvinsonden-Rasterkraftmikroskopie.* PhD Thesis, University of Stuttgart, 2015. http://elib.uni-stuttgart.de/opus/volltexte/2015/9871/

17) Sasahara, A.; Pang, C. L.; Onishi, H. Local Work Function of Pt Clusters Vacuum-Deposited on a TiO_2 Surface. *J. Phys. Chem. B* **2006**, *110*, 17584*–17588*.

18) Nishimura, T.; Iyoki, M.; Sadayama, S. Observation of Recording Pits on Phase-Change Film Using a Scanning Probe Microscope, *Ultramicroscopy* **2002**, *91*, 119–126.

19) Smit, G. D. J.; Rogge, S.; Klapwijk, T. M. Scaling of Nano-Schottky Diodes. *Appl. Phys. Lett*. **2002**, 81, 3852-3854.

20) Pérez-García, B.; Zúñiga-Pérez, J.; Muñoz-Sanjosé, V.; Colchero, J.; Palacios-Lidón, E. Formation and Rupture of Schottky Nanocontacts on ZnO Nanocolumns. Nano *Lett.* **2007**, 7, 1505-1511.

21) Schierbaum, K. D.; Fischer, S.; Torquemada, M. C.; de Segovia, J. L.; Roman, E.; Martin-Gago, J. A. The Interaction of Pt with TiO_2(110) Surfaces: A Comparative XPS, UPS, and ESD Study, *Surf. Sci.* **1996,** *345*, 261–273.

22) Erdahl, S.; Kongshaug, C.; Bjørheim, T. S.; Jalarvo, N.; Haugsrud, R.; Norby, T. Hydration of Rutile TiO_2: Thermodynamics and Effects on *n*- and *p*-Type Electronic Conduction. *J. Phys. Chem. C*, **2010**, *114*, 9139–9145.

23) Cooper, V. R.; Kolpak, A. M.; Yourdshahyan, Y.; Rappe, A. M. Supported Metal Electronic Structure: Implications for Molecular Adsorption. *Phys. Rev. B* **2005**, *72*, 081409.

24) Iwamoto, M.; Yoda, Y.; Yamazoe, N.; Selyama, *T.* Study of Metal-Oxide Catalysts by Temperature-Programmed Desorption. *J. Phys. Chem.*, **1978**, *82*, 2564–2570.

25) Kumar, C. P.; Gopal, N. O.; Wang, T. C.; Wong, M.-S.; Ke, S. C. EPR Investigation of TiO_2 Nanoparticles with Temperature-Dependent Properties. *J. Phys. Chem. B*, **2006,** 110, 5223–5229.

26) Bielanski, A.; Haber, J. *Oxygen in Catalysis*, Marcel Dekker, New York, 1991.

27) Mikulova, J.; Rossignol, S.; Barbier, J.; Duprez, D.; Kappenstein, C. Characterizations of Platinum Catalysts Supported on Ce, Zr, Pr Oxides and Formation of Carbonate Species in Catalytic Wet Air Oxidation of Acetic Acid. *Catal. Today* **2007**, *124*, 185–190.

28) Nousir, S.; Keav, S.; Barbier, J.; Bensitel, M.; Brahmi, R.; Duprez, D. Deactivation Phenomena During Catalytic Wet Air Oxidation (CWAO) of Phenol over Platinum Catalysts Supported on Ceria and Ceria-Zirconia Mixed Oxides. *Appl. Catal. B – Environmental* **2008**, *84*, 723-731.

29) Horcas, I.; Fernandez, R.; Gomez-Rodriguez, J. M.; Colchero, J.; Gomez-Herrero, J.; Baro, A. M. WSXM: A Software for Scanning Probe Microscopy and a Tool for Nanotechnology. *Rev. Sci. Instrum.* **2007**, *78*, 013705.

30) Henry, C. R. Morphology of Supported Nanoparticles. *Prog. Surf. Sci.* **2005**, *80*, 92–116.

31) Sasahara, A.; Hiehata, K.; Onishi, H. Charge Transfer Observed by a Kelvin Probe Microscope. *Catal. Surveys Asia* **2009**, *13*, 9–15.

32) Hiehata, K.; Sasahara, A.; Onishi, H. Local Work Function Analysis of Pt/TiO_2 Photocatalysts by a Kelvin Probe Force Microscope. *Nanotech.* **2007**, *18*, 084007.

33) Sasahara, A.; Pang, C. L.; Onishi, H. Probe Microscope Observation of Platinum Atoms Deposited on the $TiO_2(110)$-(1×1) Surface. *J. Phys. Chem. B* **2006**, *110*, 13453–13457.

34) Hägglund, C.; Zhdanov, V. P. Charge Distribution on and Near Schottky Nanocontacts. *Physica E, Low-Dimens. Syst. & Nanostruct.* **2006**, *33*, 296–302.

35) Jochum, W.; Sepulveda-Escribano, A.; Kramer, R. Impedance Measurements in Catalysis: Charge Transfer in Titania-Supported Noble Metal Catalysts. *Topics Catal.* **2006,** *46*, 49-55.

36) Lin, S. D.; Sanders, D. K.; Vannice M. A. Metal-Support Effects on Intramolecular Selectivity During Acetophenone Hydrogenation over Pt Catalysts. *J. Catal.* **1994**, *147*, 370–374.

37) Huzinaga, T.; Vantblik, H. F. J.; Vis, J. C.; Prins, R. XPS Investigations of Pt and Rh Supported on γ-Al_2O_3 and TiO_2. *Surf. Sci*. **1983**, *135*, 580–596.

38) Jensen, C.; Buck, D.; Dilger, H.; Bauer, M.; Phillipp, F.; Roduner, E. Maximum Hydrogen Chemisorption on KL Zeolite Supported Pt Clusters. *Chem. Commun.* **2013,** *49*, 588-590.

39) Komaya, T.; Bell, A.; Wengsieh, Z.; Gronsky, R.; Engelke, F.; King, T. S.; Pruski, M. Effects of Dispersion and Metal-Metal Oxide Interactions on Fischer-Tropsch Synthesis over Ru/TiO_2 and TiO_2-Promoted Ru/SiO_2. *J. Catal*. **1994**, *150*, 400-406.

Graphical abstract